Calcium Transients Closely Reflect Prolonged Action Potentials in iPSC Models of Inherited Cardiac Arrhythmia

C. Ian Spencer,[1,7] Shiro Baba,[1,2,7,8] Kenta Nakamura,[1,2,9] Ethan A. Hua,[1] Marie A.F. Sears,[1] Chi-cheng Fu,[1,5] Jianhua Zhang,[3] Sadguna Balijepalli,[3] Kiichiro Tomoda,[1] Yohei Hayashi,[1] Paweena Lizarraga,[1] Julianne Wojciak,[2] Melvin M. Scheinman,[2] Katriina Aalto-Setälä,[1,4] Jonathan C. Makielski,[3] Craig T. January,[3] Kevin E. Healy,[5] Timothy J. Kamp,[3] Shinya Yamanaka,[1,6] and Bruce R. Conklin[1,2,*]

[1]Gladstone Institute of Cardiovascular Disease, 1650 Owens Street, San Francisco, CA 94158, USA
[2]Departments of Medicine, Anatomy and Cellular and Molecular Pharmacology, University of California San Francisco, 500 Parnassus Avenue, San Francisco, CA 94143, USA
[3]Stem Cell and Regenerative Medicine Center, Cellular and Molecular Arrhythmia Research Program, University of Wisconsin School of Medicine and Public Health, 1111 Highland Avenue, Madison, WI 53792, USA
[4]Institute of Biomedical Technology, University of Tampere, Biokatu 12, 33520 Tampere, Finland
[5]Departments of Bioengineering, and Material Science and Engineering, University of California, Berkeley, CA 94720, USA
[6]Center for iPS Cell Research and Application, Kyoto University, 53 Kawahara-cho, Shogoin, Sakyo-ku, Kyoto 606-8507, Japan
[7]Co-first author
[8]Present address: Department of Pediatrics, Kyoto University, Kyoto 606-8507, Japan
[9]Present address: Division of Cardiology, Massachusetts General Hospital, Harvard Medical School, Boston, MA 02114, USA
*Correspondence: bconklin@gladstone.ucsf.edu
http://dx.doi.org/10.1016/j.stemcr.2014.06.003

SUMMARY

Long-QT syndrome mutations can cause syncope and sudden death by prolonging the cardiac action potential (AP). Ion channels affected by mutations are various, and the influences of cellular calcium cycling on LQTS cardiac events are unknown. To better understand LQTS arrhythmias, we performed current-clamp and intracellular calcium ($[Ca^{2+}]_i$) measurements on cardiomyocytes differentiated from patient-derived induced pluripotent stem cells (iPS-CM). In myocytes carrying an LQT2 mutation (HERG-A422T), APs and $[Ca^{2+}]_i$ transients were prolonged in parallel. APs were abbreviated by nifedipine exposure and further lengthened upon releasing intracellularly stored Ca^{2+}. Validating this model, control iPS-CM treated with HERG-blocking drugs recapitulated the LQT2 phenotype. In LQT3 iPS-CM, expressing $Na_V1.5$-N406K, APs and $[Ca^{2+}]_i$ transients were markedly prolonged. AP prolongation was sensitive to tetrodotoxin and to inhibiting Na^+-Ca^{2+} exchange. These results suggest that LQTS mutations act partly on cytosolic Ca^{2+} cycling, potentially providing a basis for functionally targeted interventions regardless of the specific mutation site.

INTRODUCTION

Seventy-five times per minute, cardiac action potentials (APs) propagate the opening and closing of multitudes of sarcolemmal ion channels. APs arise spontaneously in sinoatrial nodal cells, spreading through the myocardium in a sequence. Because APs are complex, they are vulnerable to ion channel dysfunctions, which often disrupt the heart rhythm and sometimes end in ventricular fibrillation and sudden death (Marbán, 2002).

One disorder resulting from ion-channel dysfunction, known as long-QT syndrome (LQTS), is characterized by abnormally long APs and a specific form of tachyarrhythmia, Torsade de pointes (TdP), that is precipitated by physiological triggers or by "torsadogenic" drugs. Inherited LQTS is considered rare but highly dangerous because the initial clinical presentation can be sudden death (Viskin, 1999). Physicians have difficulty treating LQTS for three principal reasons: (1) assessing the risk of cardiac events, even within the same family, is confounded because even the same mutation has differing severity in different people; (2) for some LQTS mutations, antiar-

rhythmic drugs with maintained effectiveness are lacking; and (3) the probability of TdP degenerating into ventricular fibrillation is quite low, creating uncertainty about preventative options. Underlying the incomplete penetrance of LQTS are both genetic and environmental factors (Bokil et al., 2010; Vincent, 2003). Consequently, because the triggering events—and treatments—for LQTS arrhythmias are mostly gene specific, there is an urgent need for novel methods of risk assessment (Bokil et al., 2010; Moss and Kass, 2005; Schwartz et al., 2001).

LQTS is usually diagnosed after unexplained syncopal (fainting) spells and is confirmed by electrocardiography that shows a prolonged QT interval (Jackman et al., 1990; Schwartz et al., 2001; Zareba et al., 1998). Because the QT interval represents a summation of all ventricular APs, LQTS mutations primarily affect ventricular ion channel complexes (Moss and Kass, 2005; Moss and Schwartz, 2005; Viskin, 1999). To date, the study of such mutations has centered on heterologous expression in nonmyocytes, but we can now exploit patient-derived induced pluripotent stem cells (iPSCs), offering opportunities to investigate LQTS mutations in native tissue (Bellin et al., 2013; Inoue

and Yamanaka, 2011; Itzhaki et al., 2011; Takahashi et al., 2007; Terrenoire et al., 2013).

Here, we used iPSCs to generate cardiomyocytes by reprogramming skin fibroblasts from two patients carrying dissimilar LQTS mutations. Associated with LQT2, HERG-A422T produces trafficking-defective HERG K^+ channels (K_v 11.1) that decrease the rapidly activating delayed rectifier current (I_{Kr}), which is normally responsible for the bulk of ventricular repolarization. Conversely, Na_V1.5-N406K produces a net gain of Na^+ channel function, associated with LQT3. By simultaneously measuring membrane potential (E_m) and intracellular free calcium ($[Ca^{2+}]_i$) transients, we compared the phenotypes of cardiomyocytes expressing these mutations. Our studies revealed similarly remodeled APs, with recurrent early afterdepolarizations (EADs) mirrored by comparable changes in $[Ca^{2+}]_i$ transients. Such findings may point to a Ca^{2+}-dependent, common arrhythmogenic mechanism, implying that a single therapeutic approach may be applicable to multiple forms of LQTS (Marbán, 2002; Roden and Viswanathan, 2005; Viskin, 1999).

RESULTS

Fibroblasts, iPSCs, and Cardiomyocytes Reflect the Patient Genotype

Dermal fibroblasts from LQTS patients and control subjects were reprogrammed retrovirally into iPSCs (Inoue and Yamanaka, 2011). We subsequently directed their differentiation into cardiomyocytes (iPS-CM) by published methods (Takahashi et al., 2007; Zhang et al., 2012). The myocytes formed small groups of typically two to six cells, termed microclusters, that beat spontaneously. Antibody labeling and fluorescence microscopy showed that iPS-CM had protein-expression profiles consistent with a cardiac lineage, and DNA sequencing showed they carried the patient's LQTS mutations (Figures S1 and S2 available online). Two mutation-positive clones from each patient were studied in functional assays to accommodate insertional effects in DNA.

Functional Characterization of Control and LQT2 iPS-CM

We verified that iPS-CM microclusters were functionally syncytial by observing that Fluo-4 fluorescence transients (taken to directly reflect $[Ca^{2+}]_i$) in individual cells were practically identical around the microcluster and were synchronized at a short 10 ms resolution (Figure S3). From this, we posited that whole-microcluster $[Ca^{2+}]_i$ transients (recorded by photomultiplier) could be correlated with APs recorded in any single, syncytial myocyte undergoing perforated patch clamp. By this convenient method, we compared time courses of $[Ca^{2+}]_i$ and E_m during spontaneous beating in control and LQTS myocytes.

Figure 1A (left) shows that in control iPS-CM subjected to perforated patch clamp, APs were quite brief (APD_{90}: 548 ± 55 ms, n = 14), maximum diastolic potential (MDP) was negative to −70 mV (−72 ± 1 mV) and the maximum depolarization rate (V_{max}) was brisk (45.5 ± 5.5 V/s). The spontaneous beating rhythm was regular, and $[Ca^{2+}]_i$ transients were modestly longer than APs (FTD_{90}: 759 ± 59 ms, p < 0.001). In LQT2 myocytes, APs in many microclusters were markedly prolonged and had multiple EADs. Interestingly, the $[Ca^{2+}]_i$ transients faithfully reflected this prolonged AP waveform (Figure 1A, center and right). Of the two LQT2 cell lines studied, clone A3 tended to have the longer APs and $[Ca^{2+}]_i$ transients. In unpatched A4 microclusters (70% of which showed EADs), mean $[Ca^{2+}]_i$ transient duration (at 90% amplitude) was 1.71 ± 0.31 s (n = 10)—approximately double that of controls. Results are plotted in more detail for clone A3, because both APs and $[Ca^{2+}]_i$ transients alike were prolonged more than an order of magnitude relative to control (Figure 1B). Even in single LQT2 (A3) myocytes, the shared trajectory of E_m and $[Ca^{2+}]_i$ evoked sustained contractions (Figure 1C). In both LQT2 clones, the I_{Kr} density was about 50% of control (Figure 1D), consistent with the observed AP prolongation.

The foregoing results suggest that interactions between E_m and Ca^{2+}-dependent mechanisms might further prolong the APD when I_{Kr} density is diminished. We therefore examined the APD changes associated with blocking sarcolemmal L-type Ca^{2+} channels, because I_{Kr} tends to oppose depolarizing Ca^{2+} current (I_{Ca}), especially late in the AP. Within 30 s of being exposed to 2 μM nifedipine, control APs were severely abbreviated (and beating ceased) consistent with I_{Ca} being the principal source of myocyte Ca^{2+} influx (Figure 2A). After the last AP, automaticity failed to trigger an AP upstroke (Figure 2Aii), and E_m was typically approximately −60 mV until 30 s after nifedipine was washed out (Figure 2Aiii). As in controls, exposing LQT2 (A3) iPS-CM to nifedipine abbreviated the APs, despite the I_{Kr} deficit (Figure 2B). However, whereas about 10% (2/19) of LQT2 microclusters stopped beating, most continued for at least 1 min, unless they were silenced by applying tetrodotoxin (TTX) to block Na^+ channels (Figures 2C and 2D). In LQT3 iPS-CM, we observed similar results to controls, where nifedipine caused AP shortening and arrested beating (Figure S4C). The more sustained automaticity in nifedipine-treated LQT2 iPS-CM may reflect a specific genetic process in that individual, or perhaps compensatory automaticity unmasked by the I_{Kr} insufficiency (Itzhaki et al., 2011; Xi et al., 2010).

When a cardiac AP is triggered, I_{Ca} evokes a $[Ca^{2+}]_i$ transient via Ca^{2+}-induced Ca^{2+} release (CICR) from the
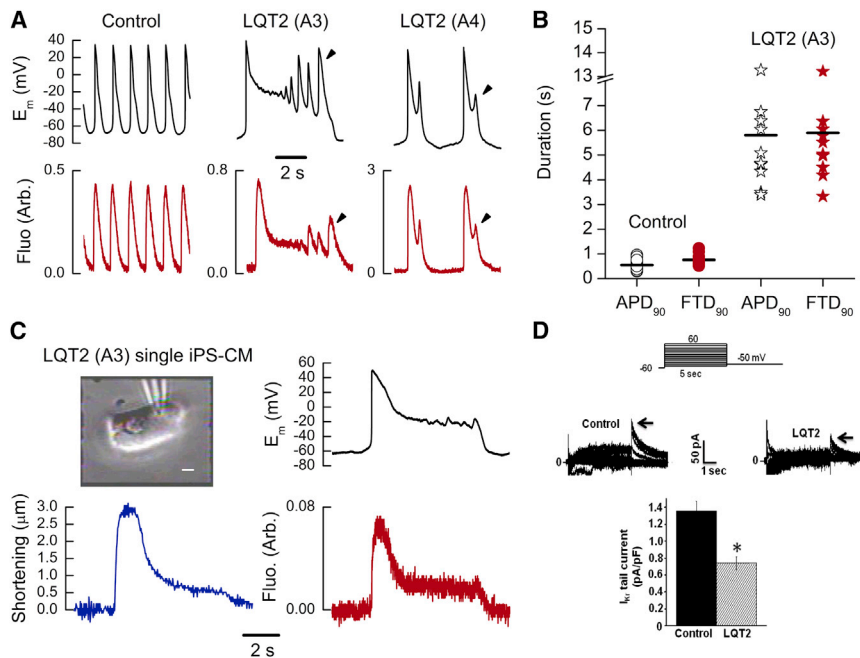
Figure 1. Electrophysiological Phenotypes in Control and LQT2 iPS-CM

(A) Upper: spontaneous APs (E_m) recorded from representative control iPS-CM and the two clones of LQT2 (as labeled). Lower: simultaneously recorded $[Ca^{2+}]_i$ transients (red) in arbitrary units (Fluo). Y axes refer to all traces to the right, and the timescale bar refers to all traces. Arrowheads point to EADs.

(B) Mean APD_{90} and simultaneously acquired FTD_{90} from control and LQT2 (A3) microclusters. Grand mean values represented by horizontal lines were: control, APD_{90} 0.55 ± 0.05 s and FTD_{90} 0.76 ± 0.06 s (n = 14); LQT2, APD_{90} 5.80 ± 0.90 s (p < 0.001 versus control) and FTD_{90} 5.89 ± 0.86 s, (p < 0.001 versus control) (n = 10).

(C) Left, top: photomicrograph of a single LQT2 (A3) iPS-CM (with patch pipette), scale bar, 10 μm. Clockwise from top right: AP from the same myocyte; $[Ca^{2+}]_i$ transient (red); cell shortening (blue trace). The signal durations coincided: APD_{90} = 6.89 s; FTD_{90} = 6.89 s; and mechanical transient duration at 90% relaxation (MTD_{90}) = 7.01 s.

(D) Representative families of E-4031-sensitive I_{Kr} tail currents (arrows) in control and LQT2 (A4) iPS-CM, and voltage protocol shown above. The histogram represents peak I_{Kr} tail-current densities for control (n = 8), and both LQT2 clones, pooled (n = 19, *p < 0.05). Error bars (SEM).

sarcoplasmic reticulum (SR). To model how CICR affects AP prolongation, we also used 10 mM caffeine to rapidly release SR-stored Ca^{2+} into the cytoplasm. In control microclusters (and in LQT2), we found that sustained caffeine applications tonically elevated $[Ca^{2+}]_i$, but inhibited beating (Figure S4A). Therefore, we employed caffeine "puffs" to modify $[Ca^{2+}]_i$ transients only briefly.

In LQT2 (A4) iPS-CM with modestly prolonged APs, applying a caffeine puff in diastole (i.e., after repolarization) triggered an AP (Figures 3A and 3B, left and center). The triggered AP and $[Ca^{2+}]_i$ transient lasted as long as the caffeine exposure (6 s), regardless of the prior spontaneous APD, and the AP lacked prominent EADs (arrow). Applying caffeine during an ongoing AP (Figures 3A and 3B, right) increased $[Ca^{2+}]_i$ and resulted in further depolarization (arrow), likely due to electrogenic Na^+-Ca^{2+} exchange (NCX) (Eisner et al., 1998). Scaled APs and $[Ca^{2+}]_i$ transients closely matched in time course, even after caffeine washout (Figure 3C, arrows), and the durations of APs affected by caffeine were markedly prolonged (Figure 3D). Further investigation by Ca^{2+} imaging showed that prolonged spontaneous and caffeine-evoked $[Ca^{2+}]_i$ transients occurred simultaneously in each cell of an LQT2 microcluster (Figure 4). Interestingly, spontaneous $[Ca^{2+}]_i$ transients were also temporarily abbreviated just after caffeine-induced release of SR Ca^{2+}, potentially indi-

cating a beat-by-beat feedback of cytosolic Ca^{2+} on E_m, modulated by Ca^{2+} extrusion.

To check whether $[Ca^{2+}]_i$ transients and APs were always prolonged together, we exposed control iPS-CM to the I_{Kr} blocker E-4031 (0.5 μM). With an increasing duration of E-4031 exposure, APs and $[Ca^{2+}]_i$ transients became longer and EADs began to occur, closely mimicking LQT2 (Figures 5A and 5B). APD_{90} and FTD_{90} were strongly correlated, and the beating rate progressively decreased, indicating that blocking I_{Kr} influenced automaticity (Figures 5B and S4B). To be sure that the effects of E-4031 were due to selective HERG channel block, we then exposed control iPS-CM to 10 μM cisapride, which has a distinct mode of action on I_{Kr} (Kamiya et al., 2008). This agent also dramatically prolonged the $[Ca^{2+}]_i$ transients, altering the waveform to resemble LQT2 and that observed under E-4031 (Figure 5C).

Gain of Function in LQT3 iPS-CM

In LQT3, APs are prolonged by increased inward Na^+ current, often late in a depolarization ($I_{Na,L}$), rather than by K^+ channel depopulation (Terrenoire et al., 2013). Nonetheless, in both LQT3 iPS-CM clones studied, the APs and $[Ca^{2+}]_i$ transients were prolonged together, analogous to our findings in LQT2 iPS-CM (Figure 6A). Between clones A1 and A3, the degree of AP prolongation was similar,
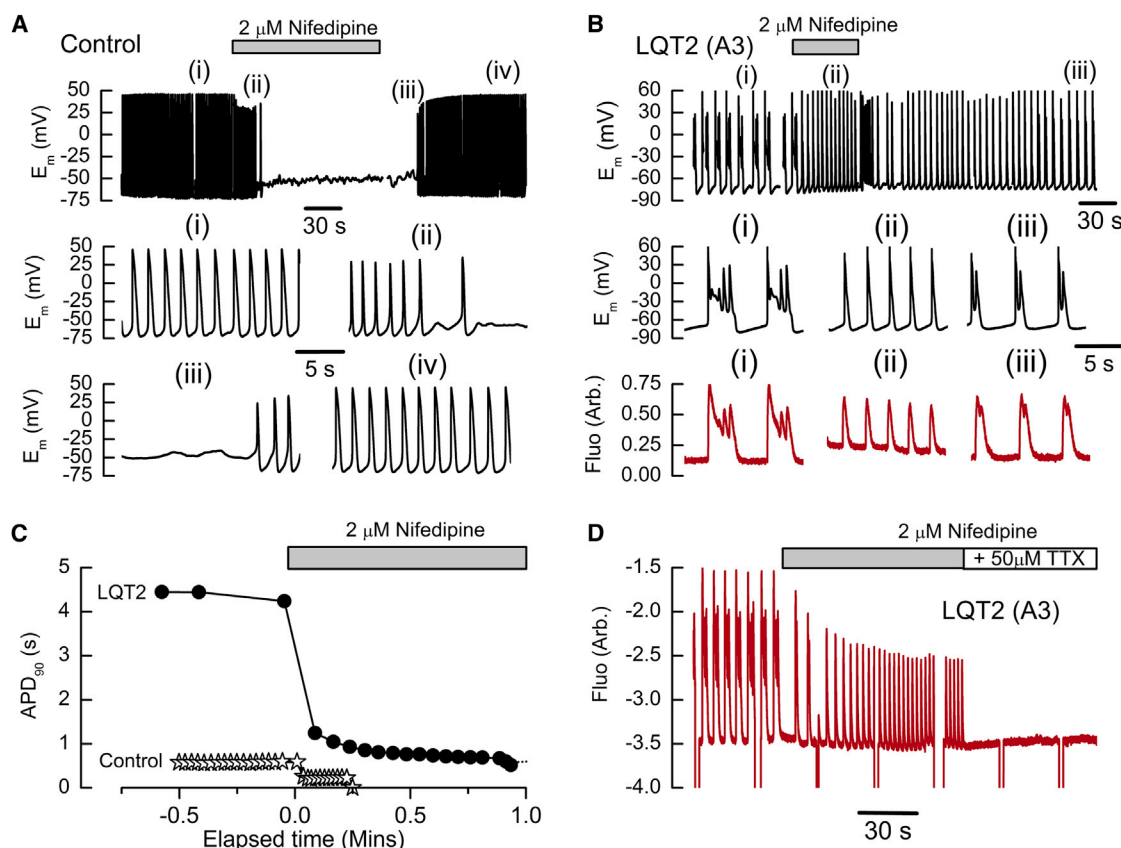
Figure 2. Effects of the Ca^{2+} Antagonist Nifedipine on Spontaneous APs and [Ca^{2+}]$_i$ Transients in Control and LQT2 iPS-CM

(A) Upper panel, time course of APs (E$_m$) during superfusion with nifedipine (gray bar) in a representative control iPS-CM microcluster, with numerals to indicate regions of interest (ROI). Center and lower panels: labeled ROI shown on an expanded scale.

(B) Upper and center panels, equivalent plots to (A), from a representative LQT2 iPS-CM cluster. Note the increase in beating rate during nifedipine exposure (gray bar). Lower panel, [Ca^{2+}]$_i$ transients (red, labeled Fluo, in arbitrary units) from ROI indicated by numerals above.

(C) APD$_{90}$ in (A) and (B) plotted against elapsed time, defined by assigning the point of nifedipine addition (gray bar) to time zero. (Control responses occurred at negative values of elapsed time.) Note that, in the LQT2 microcluster, nifedipine reduced APD$_{90}$ by 84% (to 0.71 ± 0.01 s), which was still longer than mean pre-nifedipine APD$_{90}$ in the control microcluster.

(D) Changes in [Ca^{2+}]$_i$ transients (Fluo, in arbitrary units; red trace) when an unpatched LQT2 microcluster was exposed to 2 μM nifedipine (gray bar), followed by 50 μM tetrodotoxin (TTX) in the continued presence of nifedipine (white bar), which arrested beating. Downward trace steps represent the blocking of excitation light by the shutter.

and the relationship between APD$_{90}$ and FTD$_{90}$ obeyed a single linear relation (Figure 6B). For whole-cell patched LQT3 (A3) cells, where the cytosol was dialyzed with 0.1 mM EGTA to eliminate Fluo-4 dye (Figure 6C, right), APD$_{90}$ was prolonged 14-fold relative to control (p = 0.006). Data from perforated patched myocytes were similar (center), but with shorter mean APD because somewhat fewer APs exceeded 10 s in duration.

LQT3 APs and [Ca^{2+}]$_i$ transients often incorporated long trains of EADs, causing oscillating contractions, possibly reflecting a more severe pathology (Movie S1). We therefore set out to isolate specific effects of N406K channels on APD by using the selective Na$^+$ channel blocker tetrodotoxin (TTX), to which I$_{Na,L}$ is highly sensitive (Sakmann

et al., 2000; Wu et al., 2009). In control microclusters, inhibiting I$_{Na}$ with 50 μM TTX slightly affected the beating rate and AP morphology but did not significantly shorten the mean APD$_{90}$ (Figure 6D). Moreover, in the presence of TTX, diastolic intervals shortened progressively (after an initial long pause), whereas the peak depolarization rate in the AP upstroke (V$_{max}$) continued to be depressed (beating was later abolished by adding 2 μM nifedipine). Although TTX reduced V$_{max}$ in LQT3 (A3) microclusters, it also abbreviated APD$_{90}$ (Figure 6E). During exposure to 1 μM TTX, mean APD$_{90}$ dropped significantly from 9.79 ± 4.03 to 6.30 ± 3.54 s (p = 0.003, n = 9) and V$_{max}$ fell from 54.6 ± 11.3 to 33.9 ± 8.3 V/s (p = 0.006). In response to 50 μM TTX, mean APD$_{90}$ decreased even more, from
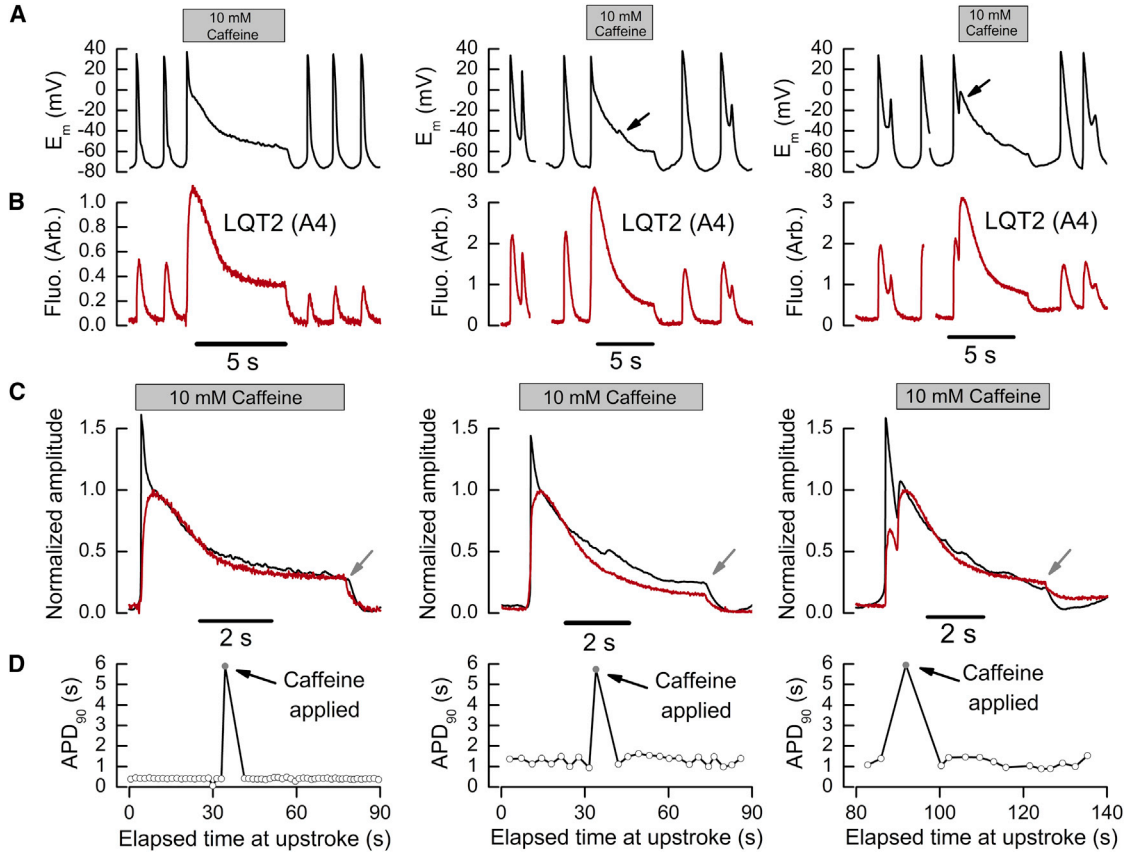
Figure 3. LQT2 AP Profiles Were Influenced by [Ca^{2+}]$_i$ Transients Stimulated by Caffeine-Induced SR Ca^{2+} Release

(A) LQT2 (A4) APs (E$_m$) with slight initial AP prolongation (left) or modest AP prolongation (center and right), before, during, and after the applications of 10 mM caffeine (gray bars). Caffeine was applied in diastole (left, center) or during the ongoing AP (right). Arrows highlight EADs.

(B) The [Ca^{2+}]$_i$ transients (red, in arbitrary units) associated with the APs of (A); gaps in the traces indicate shutter closings.

(C) Overlays of Fluo-4 fluorescence, normalized to the caffeine-induced peak and E$_m$ divided by its value at the same time point (peak of caffeine-induced [Ca^{2+}]$_i$ transient). Graphs were produced from traces in (A) and (B). Gray arrows indicate caffeine washout.

(D) APD$_{90}$ determined beat-by-beat for the entire experiments of (A). Points corresponding to APs affected by caffeine are shown in gray.

6.65 ± 1.69 to 2.08 ± 0.68 s (p = 0.008, n = 7), and V$_{max}$, decreased from 50.3 ± 12.7 to 13.6 ± 1.1 V/s (p = 0.023). Because high doses of TTX eliminate I$_{Na,L}$, the shortened APs reveal the gain-of-function in N406K channels. Nonetheless, 50 μM TTX only partially returned LQT3 APs to a duration comparable with control iPS-CM, so direct depolarization by mutant Na$^+$ channels could only account for part of the observed APD. Moreover, EADs continued to occur while LQT3 myocytes were exposed to 50 μM TTX (Figure 6E, inset) suggesting that I$_{Ca}$ and [Ca^{2+}]$_i$ also participated in the LQT3 phenotype. Consistent with this, under voltage clamp, TTX-sensitive I$_{Na,L}$ was ~35% of the total late inward current observed during 500 ms at −10 mV, whereas the remaining current was nifedipine sensitive (Figure S5). Furthermore, V$_{max}$ calculated for EADs was <10 V/s (analogous to the V$_{max}$ of AP upstrokes recorded

with 50 μM TTX present), suggesting that I$_{Na}$ was largely unavailable during the prolonged AP plateau (Figure S6).

In a previous study in rodent ventricular myocytes, we used blockers to demonstrate that NCX functionally links [Ca^{2+}]$_i$ and APD (Spencer and Sham, 2003). We therefore used a similar approach to investigate the phenotype of LQT3 iPS-CM. First, we confirmed that caffeine-induced increases in [Ca^{2+}]$_i$ prolonged the APD (in both LQT3 clones) as in LQT2 (Figure 7A). Caffeine puffs were also used to demonstrate inward NCX current (I$_{NCX}$) explicitly, under voltage clamp (Figure 7B). Interestingly, when I$_{NCX}$ was blocked with LiCl at different times during an ongoing AP, the AP was rapidly terminated and automaticity halted (Figures 7C and S4D). E$_m$ was hyperpolarized below the preceding MDP, and [Ca^{2+}]$_i$ was elevated above the usual diastolic level. Both control and LQT2 iPS-CM exposed to
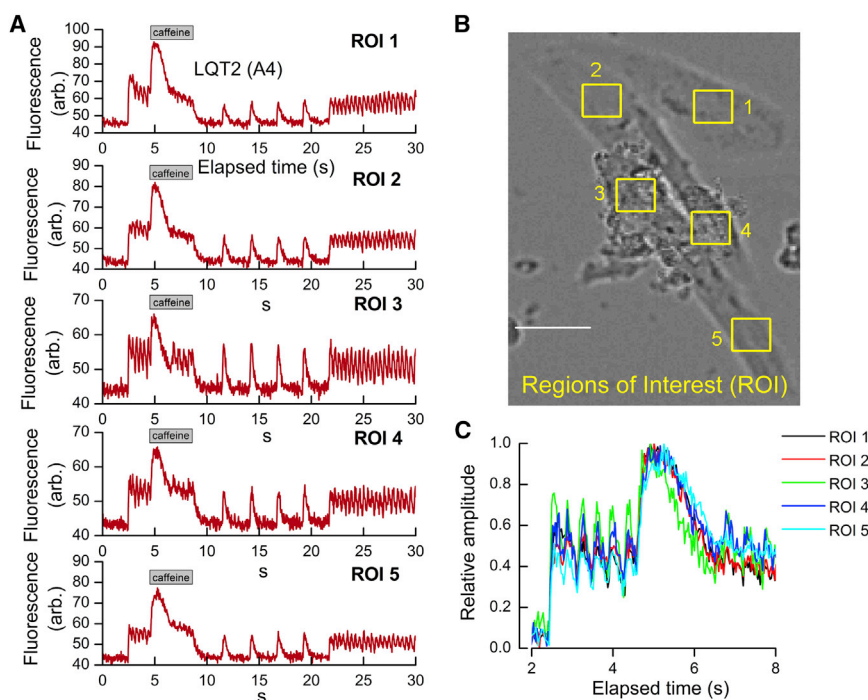
Figure 4. Comparing Spontaneous and Caffeine-Evoked $[Ca^{2+}]_i$ Transients in Individual Myocytes in an LQT2 Microcluster

(A) Fluo-4 fluorescence averaged in small, numbered regions of interest (ROIs) each within a myocyte of an LQT2 microcluster, plotted (top to bottom) versus time in the videomicrograph. During the time indicated by the gray bar, 10 mM caffeine was added to the superfusion solution.

(B) The numbered ROIs in which fluorescence was averaged (yellow rectangles) superimposed on a transmitted light image of the microcluster (scale bar, 50 μm).

(C) Overlaid time courses for each ROI at 30 ms resolution (33 frames/s in the videomicrograph). The rising phase of both spontaneous and caffeine-evoked $[Ca^{2+}]_i$ transients superimposed completely. Similar results were obtained from five different LQT2 microclusters.

LiCl exhibited similarly elevated diastolic $[Ca^{2+}]_i$ (not shown). For LQT3 cells, whose mean MDP was -86 ± 2 mV (n = 8), significant hyperpolarization to -93 ± 1 mV (p = 0.002) occurred when LiCl was applied. LiCl washout abolished the hyperpolarization, allowing beating to restart. Occasionally at this point, a delay occurred revealing the restarting of $[Ca^{2+}]_i$ transient decay (previously stalled) ahead of the upstroke of the next AP (Figure 7D, dotted line). To investigate further if hyperpolarization occurred because extracellular Li^+ caused NCX to reverse (with Ca^{2+} influx and Na^+ efflux), the experiment was repeated after omitting Ca^{2+} from the Li^+-containing solution (Figure 7E). In the nominal absence of both forward and reverse exchange, we observed that diastolic $[Ca^{2+}]_i$ was still elevated, and E_m was hyperpolarized from -79 ± 2 mV (n = 7) to -88 ± 1 mV (p = 0.004), eliminating NCX as the primary driver of these changes. Premature AP termination by Ca^{2+}-free Li^+-containing solution was associated invariably with considerable prolongation of the next spontaneous AP after returning to control Tyrode's, indicating the retention of releasable Ca^{2+} in the SR. Conversely, when SR Ca^{2+} reuptake was inhibited using 50 μM cyclopiazonic acid (CPA), a reversible blocker of the SR Ca^{2+} ATPase (SERCA), the prolonged lifetime of cytosolic Ca^{2+} could extend the AP essentially indefinitely, with occasional EADs, terminated by CPA washout (Figure 7F). These results suggest that cyclical shuttling of Ca^{2+} ions across the sarcolemma into the cell via I_{Ca} and out via NCX—with both processes producing depolarizing inward current—could contribute to the duration of APs affected by LQTS mutations (even in the absence of CPA).

DISCUSSION

This investigation focused on identifying potential mechanisms underlying LQT arrhythmias as recapitulated in myocytes generated from patient-derived iPS cells. The results complement recent investigations showing that LQTS phenotypes can be produced in human stem cell-derived myocytes (Bellin et al., 2013; Davis et al., 2012; Itzhaki et al., 2011; Lahti et al., 2012; Terrenoire et al., 2013). Although arrhythmogenic triggers are recognized to be gene related, prolonged APs are the common denominator in LQTS diseases (Schwartz et al., 2001). Our results suggest that prolonged APs may promote arrhythmia, at least partially, through Ca^{2+}-dependent mechanisms.

Though similarities in profile between the AP and $[Ca^{2+}]_i$ transient waveforms might not necessarily indicate a causal relationship, the results suggest that E_m is influenced by three major Ca^{2+}-dependent mechanisms in combination. First, blocking I_{Ca} strongly abbreviated the APs in LQT2 iPS-CM, even though AP prolongation had arisen from I_{Kr} deficiency. We attribute this to the normal presence of a sustained direct depolarization by I_{Ca}, and inward I_{NCX} during the triggered $[Ca^{2+}]_i$ transient (Eisner et al., 1998; Linz and Meyer, 2000; Spencer and Sham, 2003). Second, stimulating SR Ca^{2+} release (with caffeine) during an
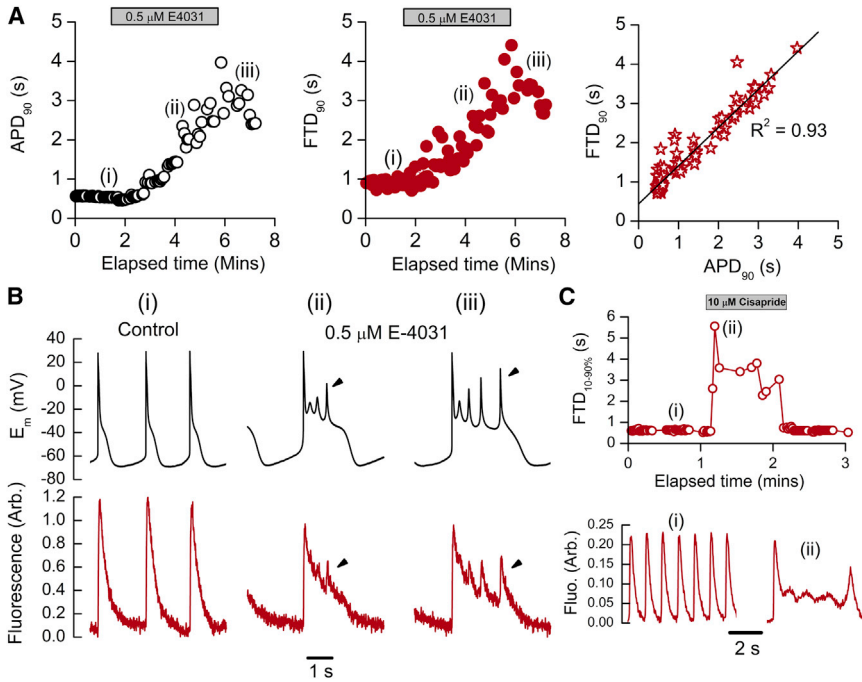
Figure 5. Control Action Potentials and [Ca^{2+}]$_i$ Transients Were Prolonged by HERG Blockers

(A) Left: APD$_{90}$ in a representative control microcluster plotted against elapsed time, before and after adding 0.5 μM E-4031 to the superfusion solution (gray bar). Center: equivalent plot of FTD$_{90}$ (in the same microcluster). Numerals identify individual traces shown in more detail below. Right: FTD$_{90}$ (from center panel) assigned to the dependent variable and plotted against APD$_{90}$ (left panel). For the linear fit: slope = 0.97 ± 0.03, intercept = 437.64 ± 38.51 ms, R^2 = 0.93.

(B) Individual APs (E$_m$, upper panels) and [Ca^{2+}]$_i$ transients (red traces in lower panels) denoted by numerals in part (A). These ROI consisted of (i) before exposure to E-4031; (ii) midway; and (iii) at maximal AP prolongation. Arrowheads indicate EADs.

(C) Plot of [Ca^{2+}]$_i$ transient duration (FTD at 10%–90%) versus elapsed time during an experiment where a control iPS-CM microcluster was exposed to 10 μM cisapride, a rapidly reversible HERG blocker. Individual, numbered [Ca^{2+}]$_i$ transients are displayed below. Mean duration increased about 10-fold during cisapride treatment (representative of six microclusters).

ongoing AP prolonged its duration, with the resulting AP reflecting the [Ca^{2+}]$_i$ waveform, and blocking SR Ca^{2+} reuptake (via SERCA) prolonged both APs and [Ca^{2+}]$_i$ transients markedly. Thus, our findings support an established mechanism whereby a portion of released Ca^{2+} is extruded, generating inward I$_{NCX}$ and thereby reactivating I$_{Ca}$ and causing EADs (January et al., 1991; January and Riddle, 1989; Makielski and January, 1998). SR Ca^{2+} reuptake facilitates further cyclic Ca^{2+} releases during EADs, particularly when E$_m$ changes are relatively undamped by repolarizing currents—as in LQTS—(Figures S6E and S7). Third, in the presence of LiCl, cytosolic Ca^{2+} appeared to equilibrate between the SR and cellular buffers, made evident by the failure of [Ca^{2+}]$_i$ to return to baseline despite membrane hyperpolarization possibly aided by limited Li$^+$-Ca^{2+} exchange (Doering et al., 1998). When not blocked by LiCl, forward NCX would likely extrude this Ca^{2+} load as part of automaticity (Zahanich et al., 2011). Indeed, depleting SR Ca^{2+} by caffeine applications briefly reset spontaneous LQT2 [Ca^{2+}]$_i$ transients to a shorter duration (Figure 4A). In both LQT2 and LQT3, the occasional prolongation of APs and Ca^{2+} transients out to tens of seconds also implies that mechanisms underlying the refractoriness and restitution of SR Ca^{2+} release are readily overridden in iPS-CM (Sobie et al., 2006). Taken together, our results show that in human LQTS myocytes (rather than drug-induced LQTS in animal models) Ca^{2+} handling is involved in prolonging

the AP, regardless of the initiating mutation. Although we encourage additional studies examining a wider range of LQTS mutations, our results suggest that antiarrhythmic treatments for LQTS could target cellular Ca^{2+} cycling, with the benefit of being genotype independent.

Safe Ca^{2+} antagonists are already used clinically, and convincing (albeit limited) evidence supports their use in LQTS diseases that resist conventional pharmacotherapy (Iseri and French, 1984; Jackman et al., 1990; Komiya et al., 2004). However, physicians appear hesitant to prescribe Ca^{2+} antagonists in LQTS for fear of triggering vasodilation, bradycardia, and further arrhythmias. Conversely, evidence from animal models favors these agents (Bailie et al., 1988; Guo et al., 2007; Thomas et al., 2007; Yamada et al., 2008). One study suggested that mere 5 mV shifts in I$_{Ca}$ activation or inactivation voltage might abolish EADs (Madhvani et al., 2011). Direct injection of MgSO$_4$ also terminates TdP effectively, but this is unsuitable for daily therapy (Johnson et al., 2001; Viskin, 1999). Interestingly, Mg^{2+} may be efficacious because it blocks both I$_{Ca}$ and SR Ca^{2+} release, but little is known about what controls the level of this ion intracellularly (Eisner et al., 1998; Iseri and French, 1984; Wang et al., 2004).

Compared to other types of LQTS, LQT3 is the most lethal (Bankston et al., 2007; Terrenoire et al., 2013; Zareba et al., 1998). Our results suggest that the LQT3 phenotype can be complex, depending directly on mutant Na$^+$ channels, and
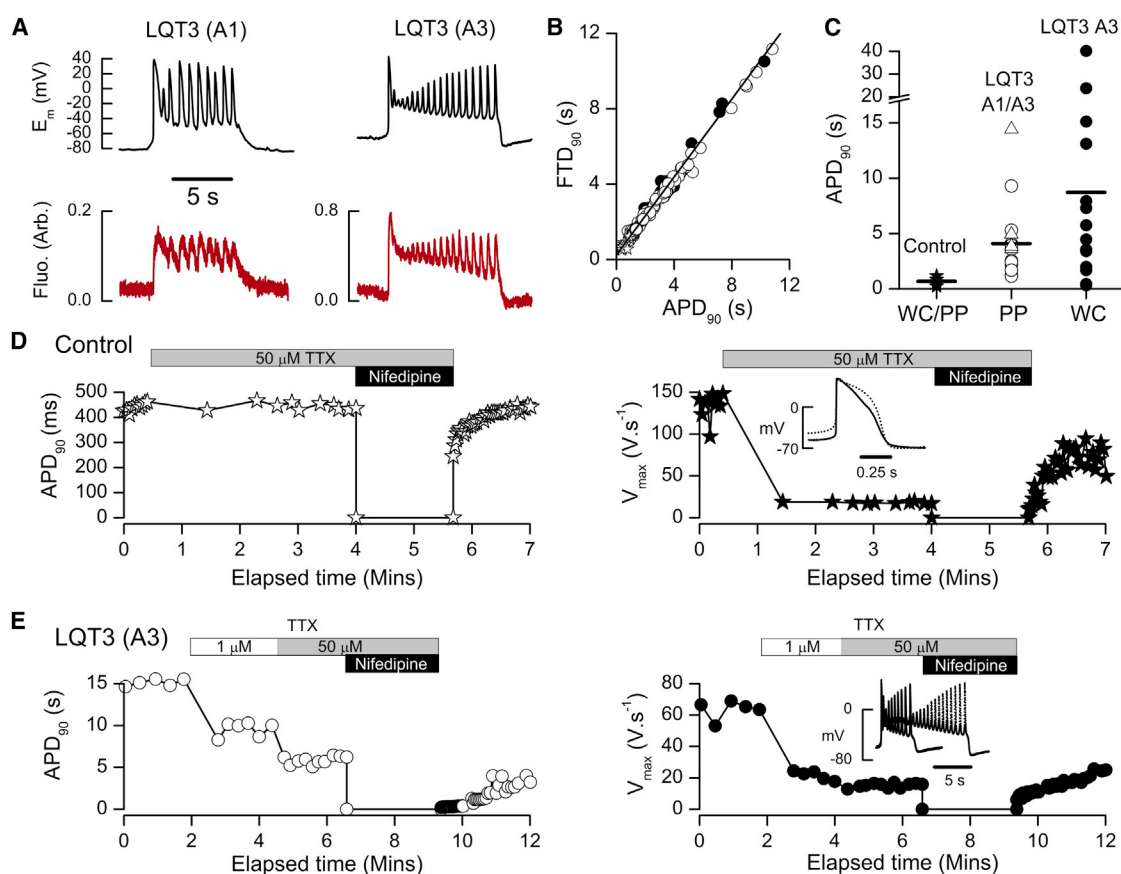
Figure 6. Phenotype and Pharmacology of LQT3 iPS-CM

(A) APs (E_m in mV, top) and $[Ca^{2+}]_i$ transients (Fluo in arbitrons, bottom) from microclusters representative of the two LQT3 clones (as labeled). Axes refer to traces to the right, and timescale bar refers to all traces.

(B) Plots of FTD_{90} versus APD_{90} from clone A1 (filled symbols) and A3 (open symbols) on the same axes, with a combined linear fit: slope = 1.03 ± 0.07, intercept = 0.25 ± 0.02, R^2 = 0.99.

(C) Dot plot showing APD_{90} from microclusters under whole cell mode (WC, closed symbols) and perforated patch clamp (PP, open symbols) in control (stars), LQT3 clone A1 (triangles), and LQT3 clone A3 (circles). Means were nonsignificantly different between LQT3 clones, or between PP and WC in any single cell type. Lines represent the overall mean in each category (combined in Table S1).

(D) Left: APD_{90} in a representative control microcluster when exposed to 50 µM TTX (gray bar), and later after adding 2 µM nifedipine (black bar). Introducing TTX initially interrupted beating for 51 s (mean pause 24 ± 7 s, n = 7), but recovery followed. Right: V_{max} for upstrokes (in the same APs) diminished from 134.5 ± 4.8 V/s to 17.9 ± 0.3 V/s in TTX. Inset: sample APs before (broken trace) and during (solid trace) TTX exposure showing that TTX altered the AP profile, leaving APD_{90} unchanged.

(E) Left: APD_{90} changes, equivalent to (D), in an LQT3 (A3) microcluster during exposure to 1 µM TTX (white bar), 50 µM TTX (gray bar), and 50 µM TTX plus 2 µM nifedipine (black bar). Right: V_{max} plot in the same LQT3 microcluster. Inset: APs before (broken trace) and during exposure to 50 µM TTX (solid trace).

partly on other conductances. I_{Ca} made up most of the measurable late inward current in LQT3 iPS-CM, substantiating the possibility that blocking this current (for which persistence is known) could be specifically useful in LQT3 (Linz and Meyer, 2000; Thomas et al., 2007). However, doubts have been expressed about whether studies using stem cell-derived myocytes are directly applicable to real-life medicine, because such cells are acknowledged to be relatively immature (Doss et al., 2012; Lieu et al., 2009). On the other hand, immaturity and spontaneous beating

in stem cell-derived myocytes has not prevented the successful development of assays for arrhythmogenesis, with some producing traces similar to ours (Abassi et al., 2012; Chang et al., 2012; Terrenoire et al., 2013). Because we could not fully constrain automaticity by electrical pacing, future studies would be aided by fuller elucidation of the underlying mechanisms or uncovering which transcription factors are required for complete iPS-CM differentiation.

Another issue relates to the choice of appropriate controls in a disease with incomplete penetrance, as highlighted by
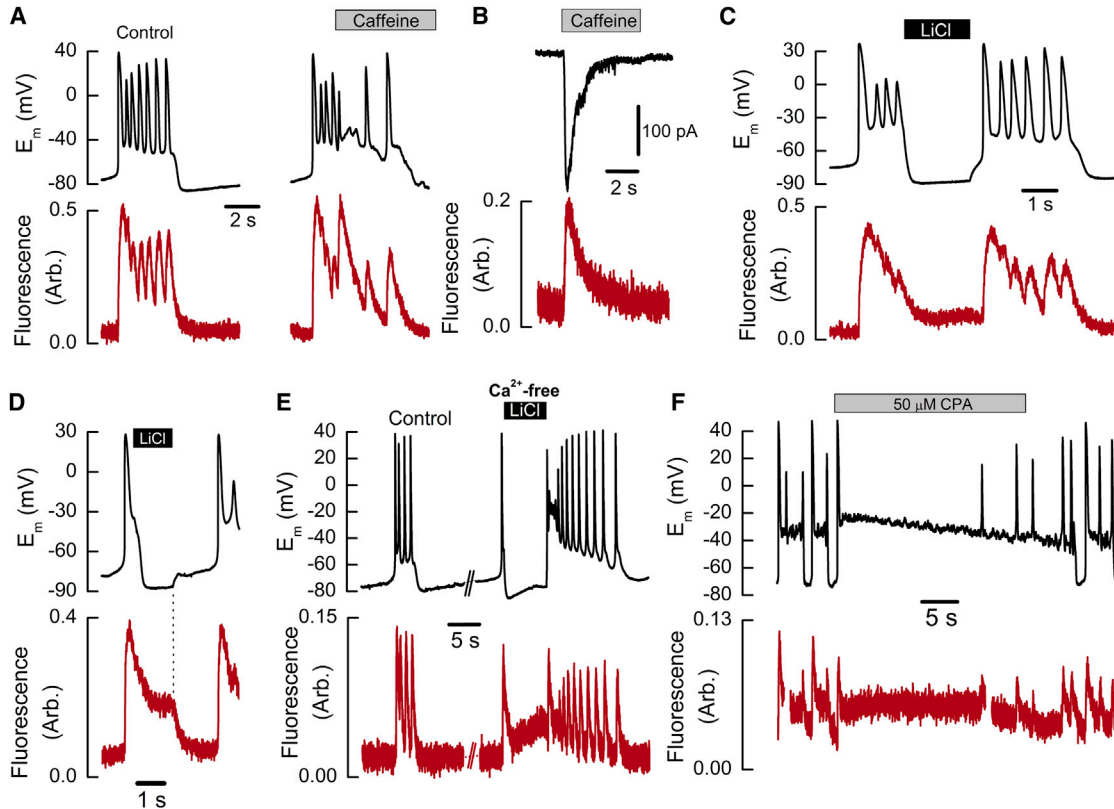
Figure 7. The Role of Cytosolic Ca^{2+} in the LQT3 Phenotype

(A) Representative LQT3 (A3) APs (top) and [Ca^{2+}]$_i$ transients (bottom) before (left) and during (right) exposure to 10 mM caffeine (gray bar). Axes refer to traces to the right, and timescale bar refers to all traces (representative of ten LQT3 (A3) and four LQT3 (A1) microclusters).

(B) Inward current (top trace) recorded, at −80 mV, from an LQT3 (A3) myocyte under perforated patch, during a caffeine puff (gray bar) that evoked SR Ca^{2+} release (lower panel). Li$^+$ sensitivity (not shown) confirmed this current as I$_{NCX}$ (n = 5).

(C) A prolonged LQT3 (A3) AP was rapidly terminated after most extracellular NaCl (except 5 mM) was replaced by with LiCl (black bar). E$_m$ was hyperpolarized, cytosolic Ca^{2+} was tonically elevated, and Li$^+$ washout evoked another AP. Results were similar in eight replicate microclusters.

(D) In a different preparation, the AP accompanying LiCl washout was more delayed, fortuitously revealing that unblocking I$_{NCX}$ produced Ca^{2+} efflux and a simultaneous depolarization (dotted line).

(E) LiCl, applied in Ca^{2+}-free extracellular solution (black bar) to additionally eliminate outward I$_{NCX}$, terminated LQT3 (A1) APs, as in (C) (n = 8). The AP associated with Li$^+$ washout was markedly prolonged relative to prior APs (labeled "control").

(F) Time course of LQT3 (A3) APs (upper panel) and [Ca^{2+}]$_i$ transients (lower, red trace) during exposure to 50 μM cyclopiazonic acid (CPA) to block SERCA (gray bar). A slowly decaying, prolonged plateau of cytosolic Ca^{2+} established a corresponding long depolarization, proceeding beyond CPA washout. Gaps in the fluorescence trace correspond to shutter closures. (Representative of five microclusters showing similar responses.)

our finding that LQT2 iPS-CM were relatively resistant to nifedipine compared to the other genotypes. Mitigating this, when we exposed control myocytes to HERG blockers, the resulting marked AP prolongation modeled LQTS in the absence of a genetic modification. Moreover, in the present studies and in some published findings, patient-derived iPS-CM lines exhibited exaggerated LQTS phenotypes as compared to clinical experience—though electrotonic and other passive effects alter the observable disease manifestations in organized tissue. Other groups found mild LQTS phenotypes, even in isogenic LQTS lines, and we found less dramatic AP prolongations in large colonies >100 myocytes (Bellin et al., 2013; Itzhaki et al., 2011; Matsa et al., 2011). Because microcluster control APDs closely matched published values from intact ventricles (Khan et al., 2010; Terrenoire et al., 2013), we suspect that a more hyperpolarized MDP may have produced a more physiologically appropriate resting state, evidenced by a generally large V$_{max}$ for AP upstrokes (see Table S1). Arguably, this led to heightened responses to LQTS mutations and to

torsadogenic drugs. Initially, we obtained MDP no deeper than −65 mV (similar to other studies), but as our differentiation technique improved, the myocytes matured developmentally (Bellin et al., 2013; Doss et al., 2012; Itzhaki et al., 2011; Zhang et al., 2012). Moreover, isolated myocytes are likely to show more severe phenotypes due to the lack of compensatory mechanisms present in the native circulatory system. Finally, in validating the functionally syncytial nature of myocyte microclusters, we were also able to show that brief APs were associated invariably with brief $[Ca^{2+}]_i$ transients, and vice versa.

Prolonged APs and EADs are typical of pharmacologically induced LQTS modeled in nonhuman hearts (Shimizu and Antzelevitch, 2000; Studenik et al., 2001; Terentyev et al., 2014), yet few such studies examined $[Ca^{2+}]_i$ transients. The lengthening of APs and $[Ca^{2+}]_i$ transients after pharmacologically blocking I_{Kr} in control iPS-CM, in direct parallel to animal studies, well corroborates our evidence from LQTS myocytes. Insights such as this suggest that benefits may accrue from routinely deriving iPS-CM from LQTS patients, both for risk assessment, and to guide treatments including whether to employ Ca^{2+} channel blockers (Terrenoire et al., 2013). In conclusion, our results contend that existing or novel Ca^{2+} antagonists (perhaps acting to shift the level of cytosolic Mg^{2+}) may help us to reduce the risk of cardiac events in the LQTS population.

EXPERIMENTAL PROCEDURES

Patient Recruitment and Characteristics

Two LQTS patients and two control individuals, who supplied written consent forms, were biopsied for dermal fibroblasts. All protocols were approved by the Committee on Human Research at the University of California, San Francisco, and conformed to the declaration of Helsinki principles. Patient 1, a 54-year-old female with LQT2 and QT_c of 493 ms on surface electrocardiogram (Figure S1A), initially presented with unexplained syncope. Genetic testing revealed a heterozygous A422T mutation (1264G > A) in the HERG K^+ channel (gene: *KCNH2*). Patient 2 was born with QT_c of 523 ms and had had a pacemaker implanted to address bradycardia and TdP (Figure S1A). A de novo N406K (1218C > A) mutation in $Na_V1.5$ (gene: *SCN5A*) led to diagnosis of LQT3. This patient unfortunately passed away during sleep, a year after her skin biopsy (aged 19). Two unrelated individuals without pre-existing disease or arrhythmia provided tissue samples for control iPSC lines. Both subjects had normal QT intervals (QTc < 450 ms). Fibroblasts from all skin biopsies were isolated, expanded and later banked under liquid nitrogen.

Production and Differentiation of iPSCs

Fibroblasts were reprogrammed and differentiated using minor modifications to the protocols listed in Supplemental Experimental Procedures (Takahashi et al., 2007; Zhang et al., 2012).

For each patient genotype, two clones were used for functional studies (named A3 and A4 in LQT2, A1 and A3 in LQT3).

Electrophysiology

At least 30 days postdifferentiation, visibly beating myocytes were dispersed by trypsinization onto fibronectin- or gelatin-coated coverslips (no. 1, CS15R, Warner Instruments). Populated coverslips were incubated in RPMI complete medium (changed every 3 days), and were transferred to the superfusion bath (Warner RC-26GLP) on a Nikon TiS inverted microscope equipped with a photomultiplier (PMT) microfluorometer (IonOptix, PMT400) and motion detector (VED, Crescent Electronics). Extracellular solutions, delivered locally near the patch-clamp electrode, were warmed to 30°C with a superfusion system (AutoMate Scientific). One myocyte of a synchronously beating microcluster was patch-clamped, while fluorescence was recorded simultaneously from the entire microcluster. Whole-cell and perforated patch clamp were employed in different experiments. An Axopatch 200B amplifier (Molecular Devices) was coupled via pClamp software (v10) to patch electrodes of 2–3 MΩ (1B-150F; WPI) filled with intracellular solution containing (mM): 120 KCl, 20 NaHEPES, 10 MgATP, 0.1 K_2EGTA, 2 $MgCl_2$, set to pH 7.1 with KOH. Perforated patch was used to record from Fluo-4 loaded myocytes after adding 240 μg/ml of amphotericin B plus 5 mM EGTA to the same pipette solution (Rae et al., 1991). If $[Ca^{2+}]_i$ transients were absent or diminished (due to patch rupture, allowing EGTA to chelate cytosolic Ca^{2+}) the experiment was terminated. Myocytes were superfused at constant flow (W2-64, Warner Instruments) with modified Tyrode's solution containing (mM): 137 NaCl, 10 NaHEPES, 10 dextrose, 5 KCl, 2 $CaCl_2$, 1 $MgCl_2$. This solution was set to pH 7.4 with NaOH. NCX was inhibited by replacing external NaCl with 137 mM LiCl, and in some experiments, $CaCl_2$ was omitted with no ionic substitution. In pharmacological experiments, drugs (caffeine, cisapride, E-4031) were obtained from Sigma or Ascent Scientific and the level of DMSO vehicle was <1%. The Axopatch amplifier was set to current clamp at zero applied current, and spontaneous APs were recorded for 30 s per data file.

Sodium current (I_{Na}) was recorded from single myocytes with high EGTA intracellular solution (as above) in which K^+ was replaced by Cs^+. Rapid delayed rectifier K^+ current (I_{Kr}) was measured after dialyzing with intracellular solution containing (mM) 130 KCl, 1 $MgCl_2$, 5 EGTA, 5 MgATP, 10 HEPES (pH 7.2 with KOH). The HERG-related tail current was quantified by difference (Figure 1D) using extracellular solution (with and without 5 μM E-4031) containing (mM): 137 NaCl, 4 KCl, 1.8 $CaCl_2$, 1 $MgCl_2$, 10 glucose, and 10 HEPES (pH 7.4 with NaOH).

Intracellular Ca^{2+} Measurements

Myocytes on coverslips were loaded with the Ca^{2+} indicator dye Fluo-4 AM, before transfer to the superfusion chamber. Loading solution contained a 1:10 mixture of 5 mM Fluo-4 AM in dry DMSO and Powerload concentrate (P10020, Invitrogen), diluted 100-fold into extracellular solution and substituted for the culture medium (5 μM final [Fluo-4]). Loading proceeded for 20 min at room temperature, followed by 20 min in dye-free extracellular solution for de-esterification before commencing recordings. Ca^{2+} transients were

recorded via a standard filter set (#49011 ET, Chroma Technology). Between sampling periods, excitation light was blocked by a shutter (CS35, Vincent Associates). Background fluorescence was recorded after removing the cell(s) from the field of view. Fluo-4 AM was purchased from Molecular Probes (Invitrogen). In some experiments, the PMT system was replaced by a high-resolution, fast charge-coupled device camera (MiCam02, SciMedia) to visualize $[Ca^{2+}]_i$ transients by videomicroscopy. Frame rates of 30–100 fps were used. Movies were analyzed with Image J software (http://rsbweb.nih.gov/ij/).

Electrophysiological Data Analysis

APs were digitized at 5 kHz and low-pass filtered at 2 kHz. Every consecutive AP (and $[Ca^{2+}]_i$ transient) was measured in each data sweep. The median number of files defining an APD phenotype was three, corresponding to 90 s of continuous recording (45 APs at 0.5 Hz). The maximum depolarization rate in the AP upstroke (V_{max}) was calculated using OriginPro 8.6 software (OriginLab) or Clampfit (pClamp 10, Molecular Devices). AP amplitude and duration, determined between the upstroke (at V_{max}) and 90% repolarization (APD_{90}), were determined using in-house analysis routines in Excel 2007 (Microsoft), with correction for a -5.6 mV liquid junction potential. Microclusters with a maximum diastolic potential (MDP) positive to -65 mV were eliminated from analysis. The time course of $[Ca^{2+}]_i$-dependent fluorescence transients was quantified as the duration at 10% amplitude (10%–90% time); or for correlation with APD_{90}, as FTD_{90}, based on the duration at 10% amplitude measured from V_{max} of the AP (coincident with the upswing of the fluorescence transient). To avoid movement artifacts in fluorescence recordings, cells and microclusters were framed by a cell-free border and bright-field images were recorded. In some experiments, cell motion was quantified from videomicrographs using an edge-detector algorithm written in LabView (National Instruments), calibrated using a stage micrometer. All statistical comparisons were performed using two-tailed, paired, or unpaired t tests. Mean values are presented with standard errors (mean ± SEM), and the numbers of replicates indicate numbers of independent microclusters constituting the mean.

SUPPLEMENTAL INFORMATION

Supplemental Information includes Supplemental Experimental Procedures, seven figures, one table, and one movie and can be found with this article online at http://dx.doi.org/10.1016/j.stemcr.2014.06.003.

AUTHOR CONTRIBUTIONS

C.I.S. designed and performed patch clamp, fluorescence, and pharmacological studies in iPS-CM and wrote the manuscript; S. Baba designed and performed fibroblast reprogramming, molecular confirmation of DNA, and protein expression in iPSCs and iPS-CM and assisted with the manuscript; K.N. recruited patients, assisted with reprogramming, advised on molecular confirmation of DNA and protein expression, and assisted with the manuscript; E.A.H. prepared and maintained iPSCs and iPS-CM cultures; M.A.F.S. referred patients, collected patient information, and prepared and maintained iPSCs and iPS-CM cultures; C.F. programmed analysis software in the LabView environment; J.Z.
advised on methods for preparing iPS-CM cultures and assisted with the manuscript; S. Balijepalli performed I_{Kr} voltage clamp electrophysiology and assisted with the manuscript; K.T. advised on reprogramming and molecular confirmation of DNA and protein expression and advised on manuscript; Y.H. advised on reprogramming and molecular confirmation of DNA and protein expression and advised on manuscript; P.L. prepared and maintained iPSCs and iPS-CM cultures; J.W. and M.M.S. referred patients, collected patient information, and assisted with the manuscript; K.A.-S. helped conceive project design, assisted with recruiting of patients, and assisted with the manuscript; C.T.J. managed iPS-CM production and voltage-clamp experiments in Wisconsin and assisted with the manuscript; J.C.M. and K.E.H. assisted with the manuscript; T.J.K. advised on iPS-CM production, electrophysiology, and all aspects of the manuscript; S.Y. advised on iPS-CM production and assisted with the manuscript; B.R.C. was overall project leader and designer, recruited patients, supervised iPS-CM production, collaborations, and assisted with the manuscript.

ACKNOWLEDGMENTS

REFERENCES

Abassi, Y.A., Xi, B., Li, N., Ouyang, W., Seiler, A., Watzele, M., Kettenhofen, R., Bohlen, H., Ehlich, A., Kolossov, E., et al. (2012). Dynamic monitoring of beating periodicity of stem cell-derived cardiomyocytes as a predictive tool for preclinical safety assessment. Br. J. Pharmacol. 165, 1424–1441.

Bailie, D.S., Inoue, H., Kaseda, S., Ben-David, J., and Zipes, D.P. (1988). Magnesium suppression of early afterdepolarizations and ventricular tachyarrhythmias induced by cesium in dogs. Circulation 77, 1395–1402.

Bankston, J.R., Yue, M., Chung, W., Spyres, M., Pass, R.H., Silver, E., Sampson, K.J., and Kass, R.S. (2007). A novel and lethal de novo

LQT-3 mutation in a newborn with distinct molecular pharmacology and therapeutic response. PLoS ONE *2*, e1258.

Bellin, M., Casini, S., Davis, R.P., D'Aniello, C., Haas, J., Ward-van Oostwaard, D., Tertoolen, L.G., Jung, C.B., Elliott, D.A., Welling, A., et al. (2013). Isogenic human pluripotent stem cell pairs reveal the role of a KCNH2 mutation in long-QT syndrome. EMBO J. *32*, 3161–3175.

Bokil, N.J., Baisden, J.M., Radford, D.J., and Summers, K.M. (2010). Molecular genetics of long QT syndrome. Mol. Genet. Metab. *101*, 1–8.

Chang, M.G., Chang, C.Y., de Lange, E., Xu, L., O'Rourke, B., Karagueuzian, H.S., Tung, L., Marbán, E., Garfinkel, A., Weiss, J.N., et al. (2012). Dynamics of early afterdepolarization-mediated triggered activity in cardiac monolayers. Biophys. J. *102*, 2706–2714.

Davis, R.P., Casini, S., van den Berg, C.W., Hoekstra, M., Remme, C.A., Dambrot, C., Salvatori, D., Oostwaard, D.W., Wilde, A.A., Bezzina, C.R., et al. (2012). Cardiomyocytes derived from pluripotent stem cells recapitulate electrophysiological characteristics of an overlap syndrome of cardiac sodium channel disease. Circulation *125*, 3079–3091.

Doering, A.E., Nicoll, D.A., Lu, Y., Lu, L., Weiss, J.N., and Philipson, K.D. (1998). Topology of a functionally important region of the cardiac Na+/Ca2+ exchanger. J. Biol. Chem. *273*, 778–783.

Doss, M.X., Di Diego, J.M., Goodrow, R.J., Wu, Y., Cordeiro, J.M., Nesterenko, V.V., Barajas-Martínez, H., Hu, D., Urrutia, J., Desai, M., et al. (2012). Maximum diastolic potential of human induced pluripotent stem cell-derived cardiomyocytes depends critically on I(Kr). PLoS ONE *7*, e40288.

Eisner, D.A., Trafford, A.W., Díaz, M.E., Overend, C.L., and O'Neill, S.C. (1998). The control of Ca release from the cardiac sarcoplasmic reticulum: regulation versus autoregulation. Cardiovasc. Res. *38*, 589–604.

Guo, D., Zhao, X., Wu, Y., Liu, T., Kowey, P.R., and Yan, G.X. (2007). L-type calcium current reactivation contributes to arrhythmogenesis associated with action potential triangulation. J. Cardiovasc. Electrophysiol. *18*, 196–203.

Inoue, H., and Yamanaka, S. (2011). The use of induced pluripotent stem cells in drug development. Clin. Pharmacol. Ther. *89*, 655–661.

Iseri, L.T., and French, J.H. (1984). Magnesium: nature's physiologic calcium blocker. Am. Heart J. *108*, 188–193.

Itzhaki, I., Maizels, L., Huber, I., Zwi-Dantsis, L., Caspi, O., Winterstern, A., Feldman, O., Gepstein, A., Arbel, G., Hammerman, H., et al. (2011). Modelling the long QT syndrome with induced pluripotent stem cells. Nature *471*, 225–229.

Jackman, W.M., Szabo, B., Friday, K.J., Fitzgerald, D.M. , Moulton, K., Wang, X., Patterson, E., and Lazzara, R. (1990). Ventricular tachyarrhythmias related to early afterdepolarizations and triggered firing: relationship to QT interval prolongation and potential therapeutic role for calcium channel blocking agents. J. Cardiovasc. Electrophysiol. *1*, 170–195.

January, C.T., and Riddle, J.M. (1989). Early afterdepolarizations: mechanism of induction and block. A role for L-type Ca2+ current. Circ. Res. *64*, 977–990.

January, C.T., Chau, V., and Makielski, J.C. (1991). Triggered activity in the heart: cellular mechanisms of early after-depolarizations. Eur Heart J *12* (*Suppl F*), 4–9.

Johnson, J.P., Jr., Balser, J.R., and Bennett, P.B. (2001). A novel extracellular calcium sensing mechanism in voltage-gated potassium ion channels. J. Neurosci. *21*, 4143–4153.

Kamiya, K., Niwa, R., Morishima, M., Honjo, H., and Sanguinetti, M.C. (2008). Molecular determinants of hERG channel block by terfenadine and cisapride. J. Pharmacol. Sci. *108*, 301–307.

Khan, J.N., Prasad, N., and Glancy, J.M. (2010). QTc prolongation during therapeutic hypothermia: are we giving it the attention it deserves? Europace *12*, 266–270.

Komiya, N., Tanaka, K., Doi, Y., Fukae, S., Nakao, K., Isomoto, S., Seto, S., and Yano, K. (2004). A patient with LQTS in whom verapamil administration and permanent pacemaker implantation were useful for preventing torsade de pointes. Pacing Clin. Electrophysiol. *27*, 123–124.

Lahti, A.L., Kujala, V.J., Chapman, H., Koivisto, A.P., Pekkanen-Mattila, M., Kerkelä, E., Hyttinen, J., Kontula, K., Swan, H., Conklin, B.R., et al. (2012). Model for long QT syndrome type 2 using human iPS cells demonstrates arrhythmogenic characteristics in cell culture. Dis. Model. Mech. *5*, 220–230.

Lieu, D.K., Liu, J., Siu, C.W., McNerney, G.P., Tse, H.F., Abu-Khalil, A., Huser, T., and Li, R.A. (2009). Absence of transverse tubules contributes to non-uniform Ca(2+) wavefronts in mouse and human embryonic stem cell-derived cardiomyocytes. Stem Cells Dev. *18*, 1493–1500.

Linz, K.W., and Meyer, R. (2000). Profile and kinetics of L-type calcium current during the cardiac ventricular action potential compared in guinea-pigs, rats and rabbits. Pflugers Arch. *439*, 588–599.

Madhvani, R.V., Xie, Y., Pantazis, A., Garfinkel, A., Qu, Z., Weiss, J.N., and Olcese, R. (2011). Shaping a new Ca²⁺ conductance to suppress early afterdepolarizations in cardiac myocytes. J. Physiol. *589*, 6081–6092.

Makielski, J.C., and January, C.T. (1998). Proarrhythmia related to prolongation of repolarization: mechanisms, monitoring, prevention and management. Card. Electrophysiol. Rev. *2*, 132–135.

Marbán, E. (2002). Cardiac channelopathies. Nature *415*, 213–218.

Matsa, E., Rajamohan, D., Dick, E., Young, L., Mellor, I., Staniforth, A., and Denning, C. (2011). Drug evaluation in cardiomyocytes derived from human induced pluripotent stem cells carrying a long QT syndrome type 2 mutation. Eur. Heart J. *32*, 952–962.

Moss, A.J., and Kass, R.S. (2005). Long QT syndrome: from channels to cardiac arrhythmias. J. Clin. Invest. *115*, 2018–2024.

Moss, A.J., and Schwartz, P.J. (2005). 25th anniversary of the International Long-QT Syndrome Registry: an ongoing quest to uncover the secrets of long-QT syndrome. Circulation *111*, 1199–1201.

Rae, J., Cooper, K., Gates, P., and Watsky, M. (1991). Low access resistance perforated patch recordings using amphotericin B. J. Neurosci. Methods *37*, 15–26.

Roden, D.M., and Viswanathan, P.C. (2005). Genetics of acquired long QT syndrome. J. Clin. Invest. *115*, 2025–2032.

Sakmann, B.F., Spindler, A.J., Bryant, S.M., Linz, K.W., and Noble, D. (2000). Distribution of a persistent sodium current across the ventricular wall in guinea pigs. Circ. Res. *87*, 910–914.

Schwartz, P.J., Priori, S.G., Spazzolini, C., Moss, A.J., Vincent, G.M., Napolitano, C., Denjoy, I., Guicheney, P., Breithardt, G., Keating, M.T., et al. (2001). Genotype-phenotype correlation in the long-QT syndrome: gene-specific triggers for life-threatening arrhythmias. Circulation *103*, 89–95.

Shimizu, W., and Antzelevitch, C. (2000). Differential effects of beta-adrenergic agonists and antagonists in LQT1, LQT2 and LQT3 models of the long QT syndrome. J. Am. Coll. Cardiol. *35*, 778–786.

Sobie, E.A., Song, L.S., and Lederer, W.J. (2006). Restitution of Ca(2+) release and vulnerability to arrhythmias. J. Cardiovasc. Electrophysiol. *17* (*Suppl 1*), S64–S70.

Spencer, C.I., and Sham, J.S. (2003). Effects of Na+/Ca2+ exchange induced by SR Ca2+ release on action potentials and afterdepolarizations in guinea pig ventricular myocytes. Am. J. Physiol. Heart Circ. Physiol. *285*, H2552–H2562.

Studenik, C.R., Zhou, Z., and January, C.T. (2001). Differences in action potential and early afterdepolarization properties in LQT2 and LQT3 models of long QT syndrome. Br. J. Pharmacol. *132*, 85–92.

Takahashi, K., Tanabe, K., Ohnuki, M., Narita, M., Ichisaka, T., Tomoda, K., and Yamanaka, S. (2007). Induction of pluripotent stem cells from adult human fibroblasts by defined factors. Cell *131*, 861–872.

Terentyev, D., Li, W., Terentyeva, R., Cooper, L., Lu, Y., Jindal, H., Peng, X., and Koren, G. (2014). Hyperphosphorylation of RyRs underlies triggered activity in transgenic rabbit model of LQT2 syndrome. Biophys. J. *106*, 561a.

Terrenoire, C., Wang, K., Tung, K.W., Chung, W.K., Pass, R.H., Lu, J.T., Jean, J.C., Omari, A., Sampson, K.J., Kotton, D.N., et al. (2013). Induced pluripotent stem cells used to reveal drug actions in a long QT syndrome family with complex genetics. J. Gen. Physiol. *141*, 61–72.

Thomas, G., Gurung, I.S., Killeen, M.J., Hakim, P., Goddard, C.A., Mahaut-Smith, M.P., Colledge, W.H., Grace, A.A., and Huang, C.L. (2007). Effects of L-type Ca2+ channel antagonism on ventric-ular arrhythmogenesis in murine hearts containing a modification in the Scn5a gene modelling human long QT syndrome 3. J. Physiol. *578*, 85–97.

Vincent, G.M. (2003). The long-QT syndrome—bedside to bench to bedside. N. Engl. J. Med. *348*, 1837–1838.

Viskin, S. (1999). Long QT syndromes and torsade de pointes. Lancet *354*, 1625–1633.

Wang, M., Tashiro, M., and Berlin, J.R. (2004). Regulation of L-type calcium current by intracellular magnesium in rat cardiac myocytes. J. Physiol. *555*, 383–396.

Wu, L., Rajamani, S., Li, H., January, C.T., Shryock, J.C., and Belardinelli, L. (2009). Reduction of repolarization reserve unmasks the proarrhythmic role of endogenous late Na(+) current in the heart. Am. J. Physiol. Heart Circ. Physiol. *297*, H1048–H1057.

Xi, J., Khalil, M., Shishechian, N., Hannes, T., Pfannkuche, K., Liang, H., Fatima, A., Haustein, M., Suhr, F., Bloch, W., et al. (2010). Comparison of contractile behavior of native murine ventricular tissue and cardiomyocytes derived from embryonic or induced pluripotent stem cells. FASEB J. *24*, 2739–2751.

Yamada, M., Ohta, K., Niwa, A., Tsujino, N., Nakada, T., and Hirose, M. (2008). Contribution of L-type Ca2+ channels to early afterdepolarizations induced by I Kr and I Ks channel suppression in guinea pig ventricular myocytes. J. Membr. Biol. *222*, 151–166.

Zahanich, I., Sirenko, S.G., Maltseva, L.A., Tarasova, Y.S., Spurgeon, H.A., Boheler, K.R., Stern, M.D., Lakatta, E.G., and Maltsev, V.A. (2011). Rhythmic beating of stem cell-derived cardiac cells requires dynamic coupling of electrophysiology and Ca cycling. J. Mol. Cell. Cardiol. *50*, 66–76.

Zareba, W., Moss, A.J., Schwartz, P.J., Vincent, G.M., Robinson, J.L., Priori, S.G., Benhorin, J., Locati, E.H., Towbin, J.A., Keating, M.T., et al.; International Long-QT Syndrome Registry Research Group (1998). Influence of genotype on the clinical course of the long-QT syndrome. N. Engl. J. Med. *339*, 960–965.

Zhang, J., Klos, M., Wilson, G.F., Herman, A.M., Lian, X., Raval, K.K., Barron, M.R., Hou, L., Soerens, A.G., Yu, J., et al. (2012). Extracellular matrix promotes highly efficient cardiac differentiation of human pluripotent stem cells: the matrix sandwich method. Circ. Res. *111*, 1125–1136.